GREEN upper envelope model for energetic electrons

Angélica Sicard, Vincent Maget, Didier Lazaro, Nicolas Balcon, Robert Ecoffet

▶ **To cite this version:**

Angélica Sicard, Vincent Maget, Didier Lazaro, Nicolas Balcon, Robert Ecoffet. GREEN upper envelope model for energetic electrons. IEEE Transactions on Nuclear Science, 2022, 69 (7), pp. 1533-1540. 10.1109/TNS.2022.3157399 . hal-03613686

HAL Id: hal-03613686
https://hal.science/hal-03613686v1

Submitted on 21 Mar 2022

HAL is a multi-disciplinary open access archive for the deposit and dissemination of scientific research documents, whether they are published or not. The documents may come from teaching and research institutions in France or abroad, or from public or private research centers.

L'archive ouverte pluridisciplinaire **HAL**, est destinée au dépôt et à la diffusion de documents scientifiques de niveau recherche, publiés ou non, émanant des établissements d'enseignement et de recherche français ou étrangers, des laboratoires publics ou privés.

GREEN upper envelope model for energetic electrons

A. Sicard, V. Maget, D. Lazaro, N. Balcon, R. Ecoffet

*

Abstract— The GREEN model is a mean model, dependent on the solar cycle, that provides proton and electron flux in the radiation belts. However, it is well known that the intensity of solar cycles is variable and the effects on proton and electron fluxes may vary from cycle to cycle. The aim of this study is therefore to develop a GREEN "Upper Envelope" model which takes into account the variation from one solar cycle to another and which gives the maximum flux for each year of the solar cycle. In this study, the "Upper Envelope" is presented for electrons only.

***Index Terms*—Electron, Model, Radiation Belt**

I. Introduction

THE well-known NASA AP8 and AE8 models [1] [2] have been the standards for a long time and have rendered huge service in satellite design. However, these models are old and need revisiting. Therefore, the AE9/AP9 (IRENE) project have existed for some time and v1.50 of this model has been available and stable since 2017 [3]. The AE9 model covers electrons from 40 keV to several MeV and the AP9 model covers protons from 100 keV to several hundred of MeV. At low energy, the IRENE model corresponds to SPM model for electrons from 1 keV to 40 keV and for protons from 1 keV to 100 keV. In parallel, ONERA have developed another global model: GREEN (Global Radiation Earth Environment) [4] [5] . This model covers a large region of space, from Low Earth Orbit (LEO) altitudes to Geostationary Earth Orbit (GEO) and above, for a wide range of energies from plasma (0.1 keV) to relativistic particles (several MeV for electrons and several hundred of meV for protons). The GREEN model provides averaged values of electron and proton fluxes as a function of the year in the solar cycle. We made the choice to focus on the dependence of the fluxes to the solar cycle and not to develop a model with confidence levels. Users can therefore get access to several different models (GREEN, AE9/AP9,…) depending on their needs. In this paper, we present the current ONERA effort to improve global models of radiation belts and in particular to upper case ones.

It is well known that the intensity of solar cycles is variable and the effects on energetic protons and electrons may vary from one cycle to the next. The purpose of this study is therefore to develop an "Upper Envelope" in the GREEN model which takes into account the variation from one solar cycle to another and which gives the maximum flux for each year of the solar cycle. Only the case for the electron population has been studied so far. The same type of “Upper Envelope” was defined in IGE-2006 model [6] . This “upper case” was based on three solar cycles of LANL-GEO data. The upper case in IGE-2006 model is described in part II. The development of the upper envelope in the GREEN model is then detailed, using NOAA-POES data [7] (part III) and Salammbô simulations [8] [9] (part IV). Finally, an example of results from the GREEN model (Mean and Upper Envelope) and comparisons with AE8 and AE9 models are shown in the last section of the paper, before the conclusions.

II. Upper Envelope in IGE-2006

An upper envelope or “upper case” is defined in the ESA standard (ECSS-E-ST-10-04) IGE-2006 model [6] . The outputs of the IGE-2006 model are the mean flux as well as the minimum and maximum flux observed from the variation of intensity from one solar cycle to another. The reader is advised to refer to Sicard-Piet et al., 2006 [6] to see in detail how this envelope was calculated.

IGE-2006 is based on three solar cycles of LANL satellites data in geostationary orbit. These data allow calculating a mean flux, depending on the solar cycle, between 1keV and 5MeV. Each year of a solar cycle is represented on a scale from year -6 to year +4 with 0 being the year of the solar minimum. Therefore, for the three solar cycles of LANL data, each year of the solar cycle (between -6 and +4) is represented by three values of electron flux: the mean flux, the upper case and the lower case. In order to obtain the upper case, for each year of the solar cycle and for each energy channel, the ratio between the maximum flux and the mean flux over the three cycles is calculated. This ratio depends on the year of the solar cycle, but only the maximum ratio over all equivalent years of solar cycles will be considered in order to have an upper envelope that does not depend on the year of the solar cycle. Fig. 1 shows this maximum ratio as a function of energy (blue diamonds). Two linear curves (one for energies from 1 keV to 1.5 MeV and the other one for energies greater than 1.5 MeV) representing an envelope bounding the data points in order to be conservative, are also shown in black in the figure. Considering only the maximum ratio over the 11

* This work was supported by CNES, the French Space Agency (4500065608-DIA94).

A. Sicard is with ONERA/DPHY, Université de Toulouse, Toulouse, France, (phone: +33-5-61-25-28-81; e-mail: angelica.sicard@onera.fr).

V. Maget is with ONERA/DPHY, Université de Toulouse, Toulouse, France, (e-mail: Vincent.maget@onera.fr).

D. Lazaro is with ONERA/DPHY, Université de Toulouse, Toulouse, France, (e-mail: didier.lazaro@onera.fr).

N. Balcon is with CNES, The French Space Agency, Toulouse, France, (email: nicolas.balcon@cnes.fr)

R. Ecoffet is with CNES, The French Space Agency, Toulouse, France, (email: robert.ecoffet@cnes.fr)

years of a solar cycle (and not a ratio depending on the year of the solar cycle) allows having a constant upper envelope whatever the year of the cycle is, and therefore allows taking into account the fact that in the space era the variability has been within a year of the 11-year nominal average.

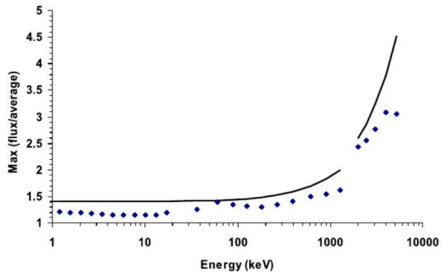

Fig. 1. Maximum (over the 11 years of a solar cycle) of the ratio of the max flux (over the three solar cycles of data) to the mean flux as a function of energy (blue diamonds). The black curves represent a fit of this max ratio taking a small margin of error.

III. Definition of the Upper Envelope in the GREEN Model using NOAA-POES Data

The idea here is to use data from the NOAA-POES satellites [7] to study the dynamics of electron fluxes from one solar cycle to the next. Coherence exists between LEO and equatorial electron measurements at high energy. Kanekal et al. [10] showed it for the first time for MeV electrons using SAMPEX data at low altitude. This property has been used previously to develop the ONERA SLOT model [11] and to deduce a radiation belt index from LEO measurements [12] . Therefore, assuming that the dynamics of electron flux is the same at low altitude as anywhere else on the field line (assuming that an equilibrium is obtained much faster along the field line than the timescale considered by the model), it is possible to calculate the ratio between max flux and mean flux from the NOAA-POES data. NOAA-POES data have many advantages: (1) as they are obtained along LEO orbits, satellites have a long lifetime (for example NOAA-POES-15 launched in May 1998 is still operational); (2) NOAA-POES constellation has been flying with quasi-similar SEM/SEM2 detectors [13] since the 80's, so long term data can be exploited and cross-calibration is then easy to handle; (3) they scan the entire field lines covering the radiation belts region, from L*=1.08 to L* values greater than 8 (GEO orbit is between L*=5.6 and L*=6.6); (4) even if the number of channels is small, detectors have well-spread energy intervals: E>30keV (E1 channel), E>100keV (E2 channel), E>300keV (E3 channel) and E>1MeV. For the last channel, it has been shown that one SEM2 proton channel (unidirectional P>6.9MeV/90°) is contaminated by electron and so allow to measure E> 1 MeV electron [14] . Therefore, the E>1MeV on SEM has been combined with the P>6.9MeV/90° on SEM2 to have long time coverage of E>1MeV electrons fluxes. Obviously, this channel has been cleaned to keep only electron data according to the Data Analysis Procedure from COSPAR-PRBEM [15] : the removal of the inner proton belt at L*<2 and the proton flares at high L* values.

It is important to keep in mind that fluxes from NOAA-POES are unidirectional fluxes and that at LEO the assumption of isotropic flux is not valid. However, the absolute value of the fluxes will not be used here but only their dynamics as a function of time. The question of anisotropy at LEO is out of the scope of the paper and will be address in further development pf the GREEN model.

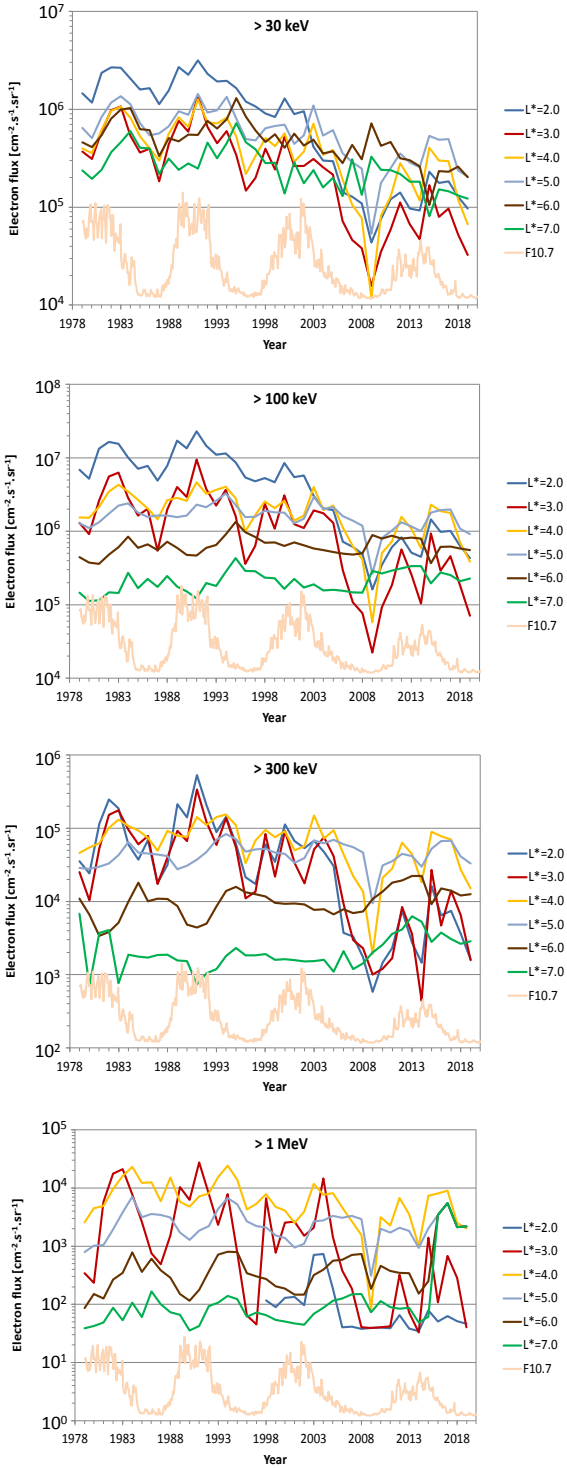

Fig. 2 Yearly averages of >30keV, >100keV, >300keV and >1MeV electron flux from NOAA-POES data as a function of the year for 6 values of L * (2.0, 3.0, 4.0, 5.0, 6.0 and 7.0).

The NOAA-POES data used in this study cover all years from 1979 to 2019, encompassing measurements from NOAA-POES-06, NOAA-POES-10, NOAA-POES-12 and NOAA-

POES-15 satellites successively. Fig. 2 represents the annual averages of >30keV, >100keV, >300keV and > 1MeV electron flux as a function of the year for 6 values of L* (2.0, 3.0, 4.0, 5.0, 6.0 and 7.0). The solar cycle variation is also plotted with F10.7 in arbitrary unit. Several observations can be made on these graphs: (1), the last solar cycle induces much smaller fluxes than the previous ones for low energies (>30keV, <100keV and >300keV) and at low L* values; (2) the dynamics of electron fluxes as a function of time increases when the energy increases and decreases as L * increases. (3) at high L* values (L*>6) and high energy (>1MeV) the maximum flux during the declining phase of the solar cycle due to magnetic storms coming from high-speed streams (coronal holes).

A decrease in low energy fluxes at low L* over the last solar cycle is quite normal: as the solar cycle was weak no strong magnetic storms happened to push the particles at low L* values. So on average the fluxes are lower. Moreover there is no decrease at high L* value for the same reasons as above: no magnetic storm pushed the particles at low L* value. Finally, at high energy (>1MeV), there were increases in electron fluxes linked to high-speed streams coming from coronal holes (always to medium-high L) [16] .

Note: Data in the > 1MeV energy range on older NOAA-POES with SEM detector (from 1979 to 1998) are not of very good quality (poorly calibrated). However, it was possible to use them anyway by recalibrating the flux from those obtained on the SEM2 instrument aboard NOAA-POES-15. On the other hand, it is important to keep in mind that the absolute value of the fluxes will not be used here but only their dynamics as a function of time.

The next step is to classify this dataset according to the years of the solar cycle. Table 1 represents the correspondence between the year and the year of the solar cycle as we used it to calculate the yearly averages of the electron fluxes as a function of the year of the solar cycle. It is important to note than some cycles only last 10 years while another last 13 years. For this one, as the minimum was longer than for the other solar cycle we choose to put three years as the minimum (2007, 2008 and 2009).

Table 1 Correspondence between year and year of the solar cycle

	Year					
Year of the solar cycle	**-6**				2001	
	-5		1981	1991	2002	2014
	-4		1982	1992	2003	2015
	-3		1983	1993	2004	2016
	-2		1984	1994	2005	2017
	-1		1985	1995	2006	2018
	0		1986	1996	2007,2008,2009	2019
	1		1987	1997	2010	
	2		1988	1998	2011	
	3	1979	1989	1999	2012	
	4	1980	1990	2000	2013	

Fig. 3 represents the yearly averages of the electron flux as a function of the year of the solar cycle for two values of L * (L*=2.5 and L*=4.5) and for the 4 energy channels (>30keV,>100keV, >300keV and >1MeV). The curves in solid lines correspond to the average fluxes over the entire period (1979-2019) and the curves in dotted lines correspond to the maximum fluxes for each year of the solar cycle over the entire time-period.

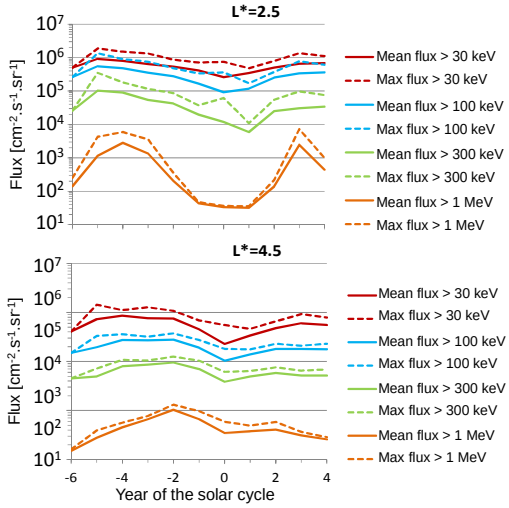

Fig. 3 Yearly averages of the electron flux from NOAA-POES as a function of the year of the solar cycle for 2 values of L * (2.5 and 4.5) and for the 4 energy ranges (>30keV,>100keV,>300keV and >1MeV). The curves in solid lines correspond to the average flux over the entire period (1979-2019) and the curves in dotted lines correspond to the maximum flux.

The third step is to calculate the ratio between the maximum flux and the average flux for each energy and each L* value. In order to eliminate any discrepancies induced by the varying solar cycle length and to margin the upper envelope estimation, only the maximum ratio for an energy and a L* value will be considered for calculating this upper envelope.

Fig. 4 represents the ratio between the maximum flux and the mean flux resulting from the analysis of the NOAA-POES data as a function of L * for 4 energy ranges (>30keV,>100keV,>300keV,>1MeV). The same ratio obtained in the case of the IGE-2006 model is also plotted in dotted lines. At the bottom a zoom of the same graph is represented. The ratio is clearly dependent on the energy and L *. It is the strongest in the region of the slot, that is to say between L * = 2 and L * = 4. This ratio is a relative variation and the high ratio in the slot region is due to the absence of particles in this region over some time periods.

The ratio reaches a maximum of 5.3 for electrons with energies > 300keV at L * = 2.4. We also observe on Fig. 4 that the ratios obtained from the NOAA-POES data between L*=5.7 and L*=7 are consistent with the ones obtained in the case of the IGE-2006 model using LANL-GEO data: the ratios from the IGE-2006 model and from NOAA-POES data are between 1.4 and 1.9. In the >100 keV and > 300 keV cases the ratios calculated from NOAA-POES data are really close to those from the IGE-2006 model. For >30 keV and >1 MeV cases the ratios are slightly different but remain on the same order of magnitude. We have no information from NOAA-POES data above 1MeV thus no comparison can be made with IGE-2006 for energies above 1 MeV.

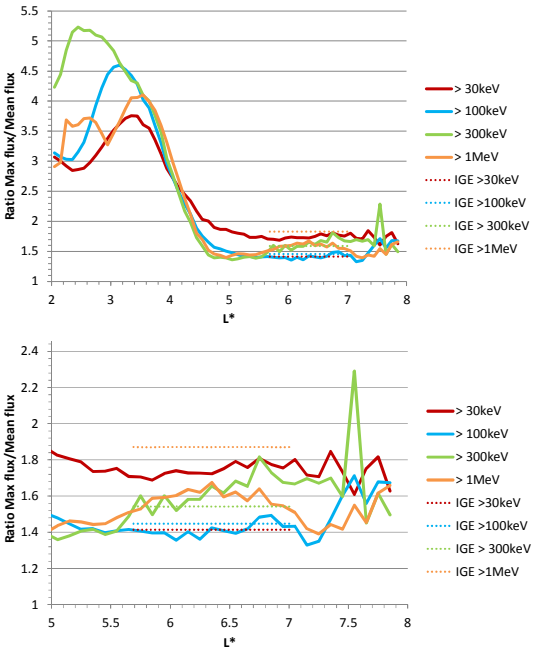

Fig. 4 Top: Ratio between maximum flux and mean flux resulting from the analysis of NOAA-POES data (1979-2019) as a function of L * for 4 energy ranges (>30keV,>100keV,>300keV,>1MeV). The same ratio obtained in the case of the IGE-2006 model is also drawn in a dotted line. Bottom: zoom of the same graph.

IV. Definition of the upper envelope from Salammbô

To compensate for the lack of information beyond 1 MeV, we used long-term simulations from the Salammbô model [8] [9] . A 3D simulation of Salammbô-electrons was performed over the same time period than for NOAA-POES data, between 1979 and 2019. Salammbô model is a physical model taking into account the following conditions:

- Radial diffusion coefficients which depend on L and on magnetic activity through K_p magnetic index $D_{LL}[s^{-1}] = 1.198 \times 10^{-14} e^{1.0362 Kp} L^{10.2}$, with an exponent of L (10.2) not far from the classical value coming from magnetic expression, and a K_p variation ($e^{1.0362Kp}$) which leads to a variation of DLL coefficients of more than 4 orders of magnitude from very quiet (K_p = 0) to very active (K_p = 9)
- Coefficients due to friction and collisions of trapped particles with the atmosphere, using the MSIS86 model [17]
- Coefficients due to wave particle interactions using the WAPI code developed by ONERA [18] taking into account Hiss and Chorus waves and the plasmapause defined by Carpenter [19]
- Boundary condition derived from NOAA-POES with a Kp dependence such as:
  - $PSD_0(K_p)$ = exp(78.814+0.3661Kp)
  - $Temp(K_p)$ = (1.2637 - 0.0917Kp)/1000
  - $Kappa(K_p)$ = 5.9606 - 0.3595Kp
  - $BoundCond(E_c,K_p)=PSD_0 (1+E_c/(Kappa.Temp))^{(-1-Kappa)}$
  - E_c is the kinetic energy of the particle

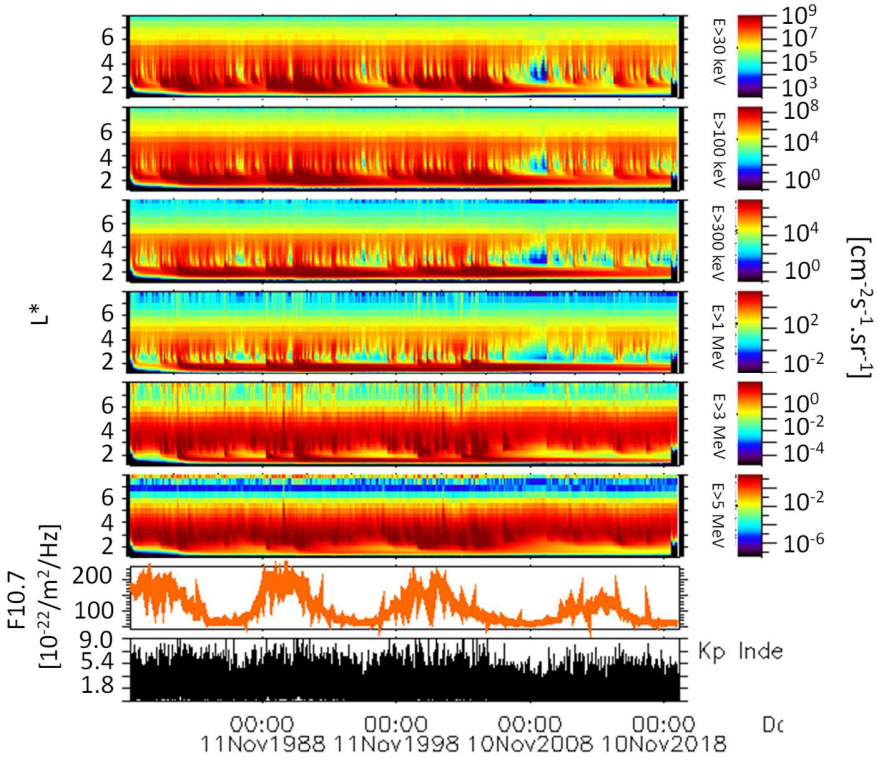

Fig. 5 Omnidirectional electron flux from Salammbô-3D model at the equator. F10.7 and Kp are also plotted.

The distribution functions calculated with Salammbô were then converted into omnidirectional flux for energies equivalent to those measured by NOAA-POES and for two additional energies in order to define the upper envelope at very high energies: >30keV, >100keV, >300keV, >1MeV, >3MeV and >5MeV.The omnidirectional fluxes resulting from Salammbô at the equator are shown in Fig. 5. The parameters F10.7 and Kp are also represented on this figure. We can clearly see the short-term dynamics associated with geomagnetic storms, but this is outside the scope of this study. Only solar cycle scale dynamics are taken into account in the GREEN model. This long-term dynamics is also visible in the electron fluxes plotted on Fig. 5.

Note: It is important to note that the Salammbô fluxes studied here are obtained at the equator while the fluxes from NOAA-POES satellites are measured in LEO. It is well known that on a same magnetic field line electron flux is much stronger near equator than at high latitude. This is why the magnitude of electron flux from Salammbô (equator) is much stronger than electron flux from NOAA-POES data (high latitude). However, in the development of GREEN and as mentioned previously, we have always assumed that even if the absolute values of electron flux are different between equator and high latitude, the long-term flux dynamics in LEO is the same as in GEO, in terms of relative variations in amplitude.

As we can see on the figure, Salammbô gives some strange results beyond L*=6 with very high fluxes at high energy (>3MeV and >5MeV) maybe due to the boundary condition which is not perfect at these high energies. Thus, we decided to use Salammbô results only up to L*=6 in the rest of the study. For L*>6 upper envelope calculated with IGE-2006 (ECSS-04c European standard for GEO) will be used.

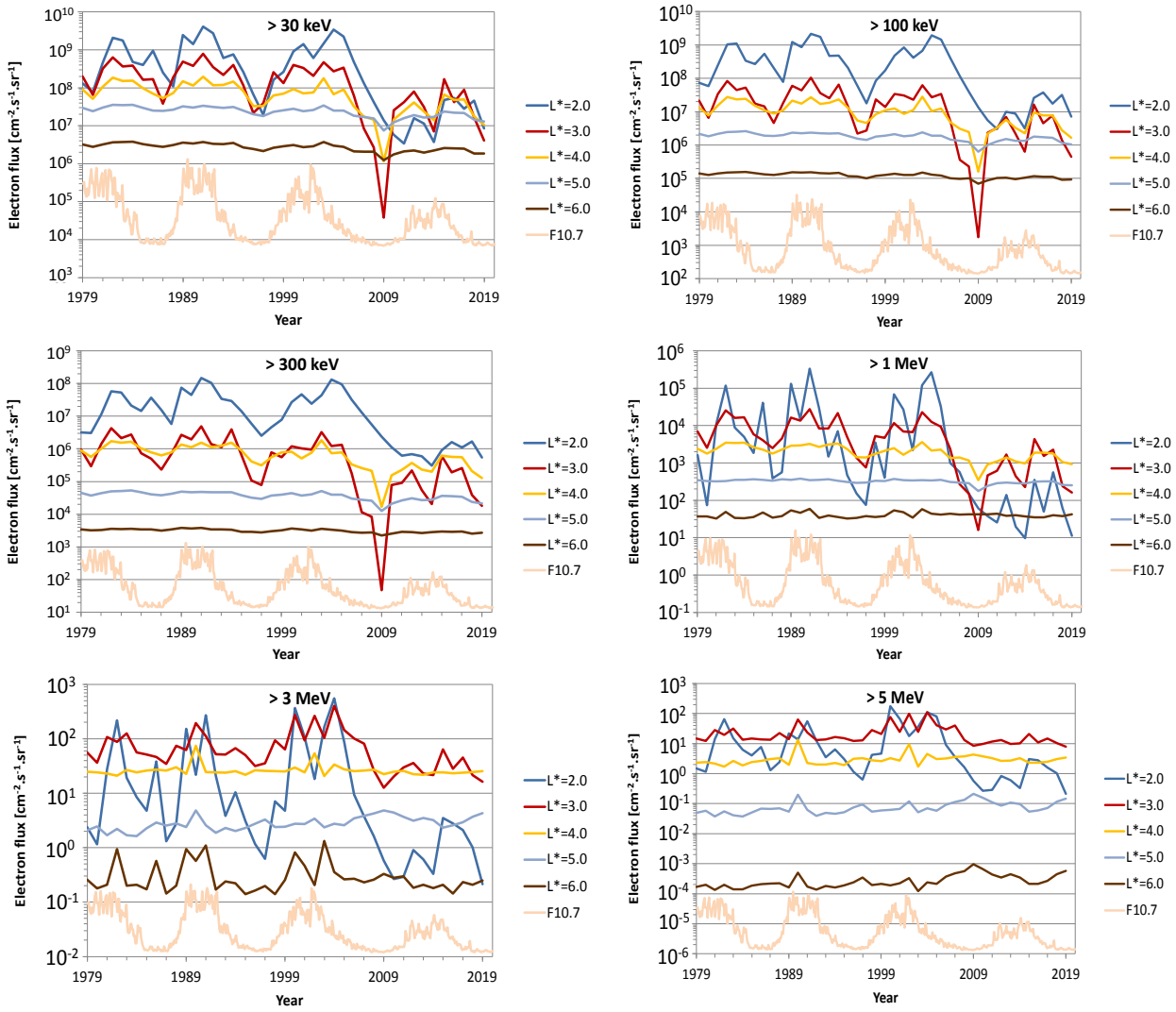

Fig. 6 Yearly averages of >30keV, > 100keV, >300keV, >1MeV, >3MeV and >5MeV electron flux from Salammbô simulation as a function of the year for 6 values of L * (2.0, 3.0, 4.0, 5.0, 6.0 and 7.0).

Fluxes from Salammbô were studied in the same way as those from NOAA-POES, described previously. Fig. 6 represents yearly averages of >30keV, >100keV, >300keV, >1MeV, >3MeV and >5MeV electron flux from the Salammbô simulation as a function of the year for 6 values of L * (2.0, 3.0, 4.0, 5.0, 6.0 and 7.0). The solar cycle variation is also plotted with F10.7 in arbitrary unit. The orders of magnitude of fluxes are higher than those from NOAA-POES because fluxes at the equator (Salammbô) are higher than fluxes at LEO (NOAA-POES).

As for NOAA-POES data Fig. 7 represents the yearly averages of the electron flux as a function of the year of the solar cycle for 2 values of L * (L*=2.5 and L*=4.5) and for the 6 energy ranges (>30keV,>100keV, >300keV, >1MeV, >3MeV and >5MeV). The curves in solid lines correspond to the average fluxes over the entire period (1979-2019) and the curves in dotted lines correspond to the maximum fluxes for each year of the solar cycle over the entire time period. Fig. 7 shows clearly that the dynamics of electron fluxes are higher inside the slot region (L*=2.5) than outside (L*=4.5).

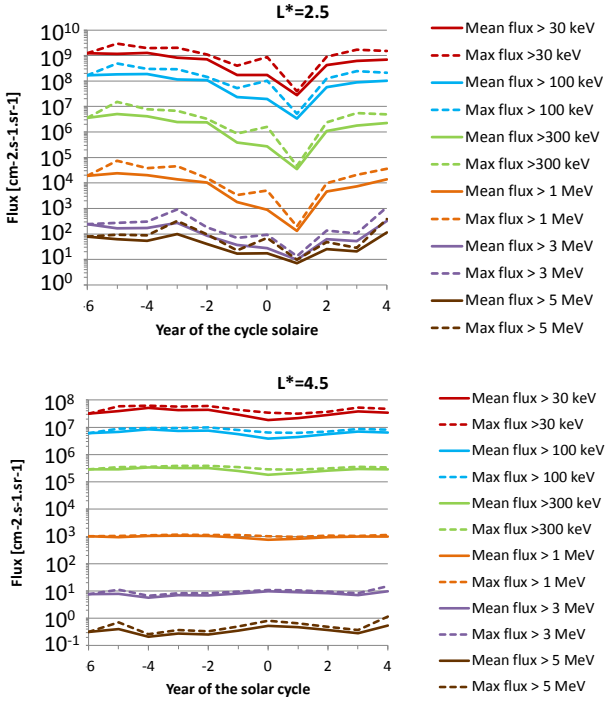

Fig. 7 Yearly averages of the electron flux from Salammbô simulations as a function of the year of the solar cycle for 2 values of L* (2.5 and 4.5) and for the 6 energy ranges (>30keV,>100keV,>300keV, >1MeV, >3MeV and >5MeV). The curves in solid lines correspond to the average flux over the period 1979-2019 and the curves in dotted lines correspond to the maximum flux.

It is really difficult to compare the dynamics of electron fluxes from NOAA-POES data and from Salammbô simulations on the previous plots. That is why, in the interest of the paper, only the ratio between maximum flux and mean flux for each energy and each L* studied in this paper will be compared thereafter.
Fig. 8 represents the ratio between the maximum flux and the average flux resulting from the analysis of Salammbô simulations (dashed lines), NOAA-POES data (full lines) and IGE-2006 results (in dotted lines) as a function of L * for 6 energy ranges (>30keV,>100keV,>300keV,>1MeV, >3MeV and >5MeV). Overall, the ratios obtained by the different analysis are consistent: ratios between 4 and 6 at low L* (L*<3.5) then a decrease up to ratios between 1 and 2 (according to NOAA-POES and Salammbô) and finally an increase of the ratio beyond L * = 5, which is greater at high energy (according to Salammbô and IGE-2006). Keep in mind that we will not used Salammbô results above L*=6 as mentioned above but the results still seem to show that the ratio increases with energy at high L* values. Fig. 9 shows these ratios for each of the first four energies (there is no data >3 MeV and > 5 MeV from NPOES data). For electrons greater than 300keV (green curves) the coherence between ratios deduced from NPOES data and those deduced from Salammbô is very good. The maximum of the ratios are at the same location (L*~2.6) and are very close (5.2 for NOAA-POES and 5.8 for Salammbô).

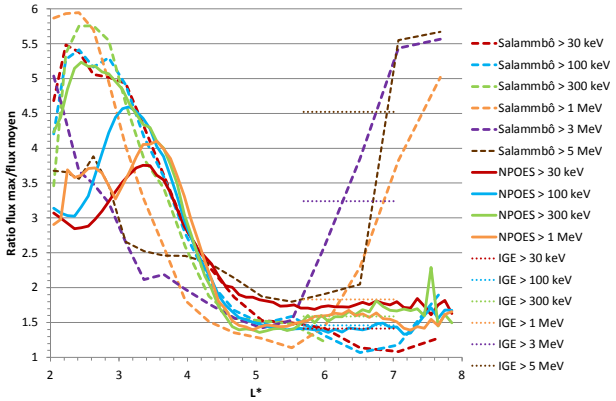

Fig. 8 Ratio between maximum flux and mean flux resulting from the analysis of Salammbô simulations between 1979 and 2019 (dashed lines), NOAA-POES data from 1979 to 2019 (full lines) and IGE-2006 results (in dotted lines) as a function of L * for 6 energy ranges (> 30keV,> 100keV,> 300keV,> 1MeV, > 3MeV and > 5MeV).

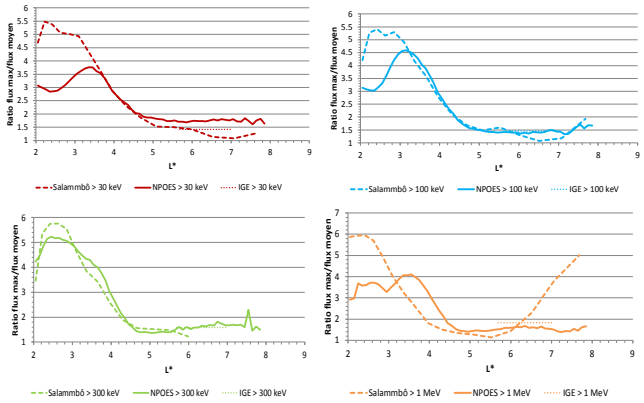

Fig. 9 Ratio between maximum flux and mean flux resulting from the analysis of Salammbô simulations between 1990 and 2019 (dashed lines), NOAA-POES data from 1979 to 2019 (full lines) and IGE-2006 results (in dotted lines) as a function of L * for 4 energy ranges (>30keV,>100keV,>300keV,>1MeV).

However, notable differences between the results from Salammbô and those from NOAA-POES should be mentioned, especially when considering the position of L * for the

maximum of the ratio Max flux /Mean flux for the three other energies. For example, at 30 keV, the maximum ratio is at L * = 2.4 according to Salammbô while it is at L * = 3.4 according to NOAA-POES. According to the NOAA-POES data, the greatest variation of the ratio is in the Slot region, while according to Salammbô, it is actually at a slightly lower L* (L*~2.5). While the profile of ratios deduced from Salammbô results is coherent between the four energies, it is really difficult to understand why this coherence does not exist for the ratio Max flux/Mean flux deduced from NOAA-POES data with a profile at 300 keV different than the three other energies. Obviously, neither the data nor the model is perfect and small differences in fluxes can lead to differences in the ratio studied here. Moreover, it is important to keep in mind that Salammbô simulations are at equator while NOAA-POES data are at high latitudes. It is really difficult to know which model or data is correct for each L* and each energy. Understanding in detail the differences between Salammbô simulations and NOAA-POES data is beyond the scope of this study.

Within the framework of our study, to define the "upper envelope" of GREEN model which takes into account the variations from one solar cycle to another, it is imperative to be conservative. Therefore, the ratio that will be integrated into GREEN model will be, for each energy and each L* value, the largest ratio between the one obtained from Salammbô, the one resulting from the analysis of the NOAA-POES data and the one resulting from the IGE-2006 model. Moreover, let's remember that the upper envelope keeps the logic used in the IGE-2006 model, i.e. that the maximum ratio from the yearly max to yearly mean only are applied. Thus, Fig. 10 represents the ratio between the maximum flux and the mean flux used to construct GREEN "Upper Envelope" model. For L*>6 ratios for upper envelope provided by IGE-2006 were used.

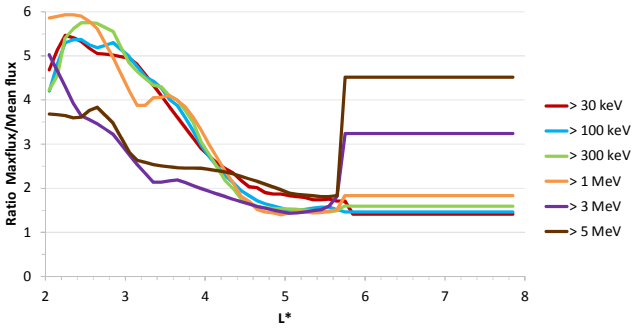

Fig. 10 Ratio between maximum flux and mean flux used to construct GREEN Upper Envelope as a function of L * for 6 energy ranges (>30keV,>100keV,>300keV,>1MeV, >3MeV and >5MeV).

V. Upper Envelope in GREEN and Examples of Results

Finally, in order to obtain the upper envelope of electron flux in GREEN, the ratios defined previously have been multiplied by the mean electron fluxes provided by GREEN. In more detail, for each point of a given orbit and each energy asked by the user the mean flux is first calculated with the GREEN model. Then according to the magnetic coordinates and the energy, the ratio is interpolated is the (L*,energy) grid plotted on Fig. 10. The mean flux is then multiplied by this ratio in order to obtain the upper flux for each point of the orbit and each energy. Therefore, we can now calculate the average electron flux on different types of orbits (MEO, GEO, EOR,…) from GREEN Mean and GREEN "Upper envelope". Fig. 11 represents the mean spectra of electrons along a GPS-like orbit in 2003 (in solar maximum) at the top, along a GEO for 11 years in the middle and along an equatorial EOR (from LEO to GEO; altitude minimum: 214km and altitude maximum : 53000km) orbit at the bottom, from GREEN Mean (in blue) and GREEN "Upper Envelop" (in red). The ratio between the averaged upper flux and the average mean flux is also represented, in grey.

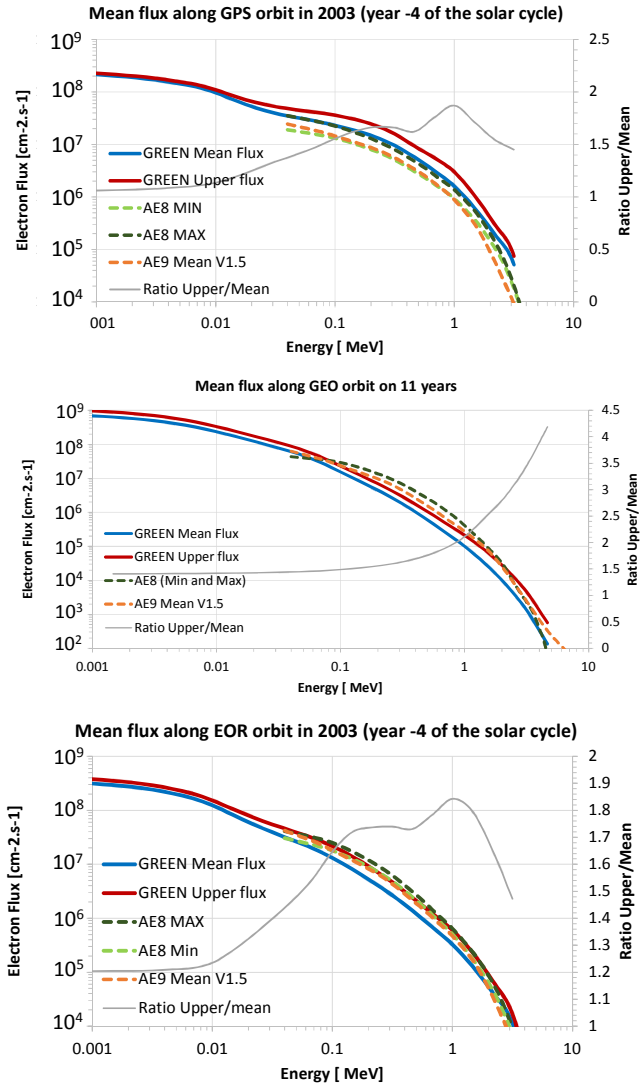

Fig. 11 Average electron spectra for a MEO orbit (GPS like orbit) in 2003 (solar maximum) from average GREEN-e (in blue) and GREEN "Upper Envelope" (in red). The ratio between the two spectra is also represented, in gray. Results from AE8 MIN (in light green), AE8 MAX (in dark green) and AE9 Mean (in orange) are also plotted.

Results from AE8 MIN (in dashed light green), AE8 MAX (in dashed dark green) and AE9 Mean (in dashed orange) are also plotted. It can be observed that the ratio between the mean flux and the "Upper envelope" flux increases with energy and can reach a factor of 2 at 5 MeV for GPS-like orbit, a factor of 4.2

at 5MeV for GEO and a factor of 1.9 at 1.5MeV for equatorial EOR orbit. If we compare GREEN "Upper Envelope" results with AE8 and AE9, Fig. 11 shows that electron fluxes provided by the AE8/9 models are slightly lower than GREEN results in the case of GPS-like orbit, slightly higher than GREEN results in the case of GEO and really close in the case of equatorial EOR orbit.

VI. Conclusion

GREEN is a mean model of electron and proton flux depending on the year of the solar cycle. In this paper, we have described a new version of GREEN that provides mean flux but also an "upper envelope". This upper envelope takes into account the variation of electron flux from one solar cycle to another in the same way the IGE-2006 model has been done for GEO orbit. To define this upper envelope NOAA-POES data between 1979 and 2019 have been analyzed and ratios between mean yearly flux and maximum yearly flux have been defined. In parallel similar ratios have been calculated using Salammbô simulations between 1990 and 2019 and IGE-2006 results. In order to be conservative the highest ratio was selected for each energy and each L* value. Then the mean fluxes in GREEN were multiplied by these ratios to obtain the GREEN upper envelope. The upper envelope is defined only for electron between 30keV and 5MeV flux. Comparison of results from GREEN "Upper Envelope" and other models like AE8 and AE9 shows that for some orbits fluxes from GREEN "Upper Envelope" can be slightly higher than those models while it can be slightly lower for other orbits.

The "Upper Envelope" is part of the GREEN-V4 model and will be available in the OMERE Tool [20] .

Acknowledgment

We thank the NOAA's National Geophysical Data Center (NGDS) for providing NOAA POES data.

References

[1] D. M. Sawyer and J. I. Vette, "AP-8 trapped proton environment for solar maximum and solar minimum" in NSSDC/WDC-A-R1S 76-06, Natl. Space Sci. data Cent., Greenbelt, MD, USA, Dec.1976.

[2] J. I. Vette, "The AE-8 Trapped Electron Model Environment", NSSDC/WDC-A-R1S 91-24, Natl. Space Sci. Data Cent., Greenbelt, MD, USA, Dec. 1991.

[3] G. P. Ginet, T. P. O'Brien, S. L. Huston, W. R. Johnston, T. B. Guild, R. Friedel, C. D. Lindstrom, C. J. Roth, P. Whelan, R.A. Quinn, D. Madden, S. Morley and Y.-J. Su, "AE9, AP9 and SPM: New models for Specifying the Trapped Energetic Particles and Space Plasma Environment", *Space Sci. Rev*., 179, pp 579-615, March 2013.

[4] A. Sicard, D. Boscher, S. Bourdarie, D. Lazaro, D. Standarovski, R. Ecoffet, "GREEN: the new Global Radiation Earth ENvironment model (beta version)," Annales of Geophysicae, vol. 36, pp 953-967, June 2018.

[5] A. Sicard, D. Boscher, D. Lazaro, S. Bourdarie, D. Standarovski and R. Ecoffet, "New Model for the Plasma Electrons Fluxes (Part of GREEN Model)", in IEEE Transactions on Nuclear Science, vol. 66, no. 7, pp. 1738-1745, June 2019.

[6] A. Sicard-Piet, S. Bourdarie, D. Boscher, R. H. Friedel, M. Thomsen, T. Goka, H. Matsumoto, and H. Koshiishi, "A new international geostationary electron model: IGE-2006, from 1 keV to 5.2 MeV", *Space Weather*, 6, S07003, pp 1-13, July 2008.

[7] D.S. Evans, M.S. Greer, "Polar Orbiting Environmental Satellite Space Environment Monitor - 2: Instrument Descriptions and Archive Data Documentation", NOAA Technical Memorandum, Space Environment Center, Boulder, 2000.

[8] T. Beutier, and D. Boscher, "A three-dimensional analysis of the electron radiation belt by the Salammbô code", *J. Geophys. Res.*,100 (A8), pp 14853–14861, Aug. 1995.

[9] D. Herrera, V. Maget and A. Sicard-Piet, "Characterizing magnetopause shadowing effects in the outer electron radiation belt during geomagnetic storms", *J. Geophys. Res. Space Physics*, 121, pp 9517– pp9530, Sept. 2016.

[10] S.G. Kanekal, D.N. Baker, J.B. Blake, "Multisatellite measurements of relativistic electrons: global coherence", *J. Geophys. Res*., vol. 106-A12, pp. 29721-29732, Dec. 2001.

[11] A. Sicard-Piet, D. Boscher, D. Lazaro, S. Bourdarie, G. Rolland, "A new ONERA-CNES Slot Electron Model", *IEEE Trans. Nuc. Sci*., vol. 61-4, pp. 1648-1655, Oct. 2014

[12] D. Lazaro, D. Boscher, S. Bourdarie, A. Sicard-Piet, G. Rolland, R. Ecoffet, E. Lorfèvre, "Radiation Belt Activity and Solar Proton Event Alarm", *IEEE Trans. Nuc. Sci*., vol. 61-4, pp. 1671-1678, Feb. 2014.

[13] V.J. Raben, D.S. Evans, H.H. Sauer, S.R. Sahm, M. Huynh, "TIROS/NOAA satellite space environment monitor data archive documentation: 1995 update," Nat. Ocean. Atmos. Admin., Silver Spring,MD, USA, Tech. Memo. ERL SEL-86, Feb. 1995.

[14] D. Boscher , S. Bourdarie, V. Maget, A. Sicard , G. Rolland, and D. Standarovski, "High-Energy Electrons in the Inner Zone", *IEEE Trans. Nuc. Sci.*, vol. 65, pp 1546-1552, April 2018.

[15] https://prbem.github.io/documents/Standard_Data_Analysis.pdf

[16] R. B. Horne, M. Phillips, S.A. Glauert, N. P. Meredith, A. D. Hands, K. Ryden, and W. Li, "Realistic worst case for a severe space weather event driven by a fast solar wind stream", *Space Weather*,16, pp 1202–1215, Aug. 2018.

[17] A. E. Hedin, "MSIS-86 Thermospheric Model", *J. Geophys. Res*., 92(A5), pp 4649– 4662, May 1987.

[18] A. Sicard-Piet, D. Boscher, R.B. Horne, N. P. Meredith and V. Maget, V., "Effect of plasma density on diffusion rates due to wave particle interactions with chorus and plasmaspheric hiss: extreme event analysis", *Ann. Geophys*., 32, pp 1059–1071, Aug. 2014.

[19] D. L. Carpenter and R. R. Anderson, "An ISEE/whistler model of equatorial electron density in the magnetosphere", *J. Geophys. Res*., 97, pp 1097-1108, Feb. 1992.

[20] https://www.trad.fr/en/space/omere-software/